

1 Incorporation of Advanced Aerosol Activation Treatments into CESM/CAM5: Model
2 Evaluation and Impacts on Aerosol Indirect Effects

3 Brett Gantt^{1*}, Jian He¹, Xin Zhang¹, Yang Zhang¹, and Athanasios Nenes^{2,3}

4 ¹Department of Marine, Earth, and Atmospheric Sciences, North Carolina State University,
5 Raleigh, NC

6 ²School of Earth and Atmospheric Sciences, Georgia Institute of Technology, Atlanta, GA

7 ³School of Chemical and Biomolecular Engineering, Georgia Institute of Technology, Atlanta,
8 GA

9 *now at: Atmospheric Modeling and Analysis Division, National Exposure Research Laboratory,
10 US Environmental Protection Agency, Research Triangle Park, North Carolina, USA

11 Corresponding author: yang_zhang@ncsu.edu

12 **Abstract**

13 One of the greatest sources of uncertainty in the science of anthropogenic climate change
14 is from aerosol-cloud interactions. The activation of aerosols into cloud droplets is a direct
15 microphysical linkage between aerosols and clouds; parameterizations of this process link
16 aerosol with cloud condensation nuclei (CCN) and the resulting indirect effects. Small
17 differences between parameterizations can have a large impact on the spatiotemporal
18 distributions of activated aerosols and the resulting cloud properties. In this work, we
19 incorporate a series of aerosol activation schemes into the Community Atmosphere Model
20 version 5.1.1 within the Community Earth System Model version 1.0.5 (CESM/CAM5) which
21 include factors such as insoluble aerosol adsorption and giant cloud condensation nuclei (CCN)
22 activation kinetics to understand their individual impacts on global-scale cloud droplet number
23 concentration (CDNC). Compared to the existing activation scheme in CESM/CAM5, this series
24 of activation schemes increase the computation time by ~10% but leads to predicted CDNC in
25 better agreement with satellite-derived/in-situ values in many regions with high CDNC but in
26 worse agreement for some regions with low CDNC. Large percentage changes in predicted
27 CDNC occur over desert and oceanic regions, owing to the enhanced activation of dust from
28 insoluble aerosol adsorption and reduced activation of sea spray aerosol after accounting for
29 giant CCN activation kinetics. Comparison of CESM/CAM5 predictions against satellite-
30 derived cloud optical thickness and liquid water path shows that the updated activation schemes

31 generally improve the low biases. Globally, the incorporation of all updated schemes leads to an
32 average increase in column CDNC of 150% and an increase (more negative) in shortwave cloud
33 forcing of 12%. With the improvement of model-predicted CDNCs and better agreement with
34 most satellite-derived cloud properties in many regions, the inclusion of these aerosol activation
35 processes should result in better predictions of radiative forcing from aerosol-cloud interactions.

36 1. Introduction

37 The interaction between cloud and aerosols is among the most uncertain aspects of
38 anthropogenic climate change (Boucher et al., 2013). By serving as cloud condensation nuclei
39 (CCN), anthropogenic aerosols can increase droplet number concentration and enhance the
40 albedo of liquid-phase clouds (Twomey, 1974, 1977). In reducing droplet size, anthropogenic
41 CCN can inhibit drizzle production under certain conditions and lead to increased liquid water
42 content, cloud lifetime, and cloud albedo (Albrecht, 1989). These two processes are referred to
43 as the radiative forcing from aerosol-cloud interactions and adjustments and collectively
44 constitute the effective radiative forcing from aerosol-cloud interactions in the Fifth Assessment
45 Report from the Intergovernmental Panel on Climate Change (Boucher et al., 2013). An
46 important aspect of aerosol-cloud interactions involves the process of aerosol activation into
47 droplets (also referred to as droplet nucleation), which describes the growth of aerosols into
48 cloud droplets. Although Köhler theory (Köhler, 1936) accurately predicts the activation of
49 particles at a given maximum supersaturation, it is the determination of the maximum
50 supersaturation that is the greatest source of uncertainty (Ghan et al., 2011). The earliest
51 representations of droplet nucleation in climate models used empirical relationships between
52 CDNC and sulfate mass concentration (Boucher and Lohmann, 1995) or aerosol number
53 concentration (Jones et al., 1994). Despite relatively strong relationships between CDNC and
54 these aerosol parameters in several environments (Leitch et al., 1992; Martin et al., 1994;
55 Ramanathan et al., 2001), the empirical relationships do not explicitly account for the
56 dependence of the droplet nucleation on aerosol size distribution, aerosol composition, or updraft
57 velocity and therefore are limited in their ability to accurately predict CDNC on a global scale.

58 Physically-based parameterizations of aerosol activation or droplet nucleation are
59 designed to quickly provide the number of aerosols activated into cloud droplets as a function of
60 the aerosol number size distribution, chemical composition, and environmental conditions. One
61 of the most widely-used parameterizations describing aerosol activation, Abdul-Razzak and
62 Ghan (2000) (hereto referred as AR-G00), is based on the work of Abdul-Razzak et al. (1998)
63 and derives a semi-empirical treatment of supersaturation by adjusting coefficients on
64 physically-based terms to achieve agreement with numerical simulations. By parameterizing
65 aerosol activation in terms of a critical supersaturation (Twomey, 1959) and critical radius within
66 a lognormal aerosol size distribution (Ghan et al., 1993), Abdul-Razzak et al. (1998) obtained an

67 activation parameterization in terms of all of the parameters of the aerosol size distribution
68 whose activated fraction is within 10% difference from that of a numerical model for most
69 conditions. AR-G00 updated Abdul-Razzak and Ghan (1998) (which applied to a single
70 lognormal aerosol mode with uniform chemical composition) by enabling its application to an
71 aerosol population represented by multiple lognormal modes, each with a uniform bulk
72 hygroscopicity determined by an internal mixture of chemical components within each mode.
73 As air quality and climate models often characterize aerosols by multiple lognormal modes, AR-
74 G00 has been widely included in many models (see Table 3 in Ghan et al. (2011) for summary).

75 Another widely-used activation parameterization, Fountoukis and Nenes (2005) (hereto
76 referred as FN05), is based on Nenes and Seinfeld (2003) and includes explicit calculations of
77 mass transfer, condensation coefficient, integration over the aerosol size distribution, and kinetic
78 limitations. In order to maintain computational efficiency, the parameterization of Nenes and
79 Seinfeld (2003) split the aerosol population (defined in terms of a sectional size distribution) into
80 two groups: 1) those with diameters that activate near the maximum supersaturation and 2) those
81 with diameters that do not activate near the maximum supersaturation. FN05 updated this
82 parameterization to account for a lognormal aerosol size distribution and size-dependent mass
83 transfer coefficient of water vapor to droplets; it also addresses some of the limitations of AR-
84 G00, especially for conditions when kinetic limitations on droplet nucleation are expected.
85 When strong kinetic limitations occur, the maximum supersaturation is not the same as the
86 critical supersaturation (defined as the saturation at which a particle radius will grow beyond the
87 equilibrium size at the maximum supersaturation). Under these conditions, the relationship
88 between maximum and critical supersaturation is determined empirically in FN05 from
89 numerical simulations for a range of conditions. Another unique feature of FN05 is its ability to
90 account for the influence of gas kinetics on the water vapor diffusivity. This influence depends
91 on particle size and on the value of the condensation coefficient. Fountoukis and Nenes (2005)
92 found that an average value of the diffusivity over an appropriate size range can account for the
93 influence of gas kinetics on droplet nucleation. By expressing the solution in terms of the
94 condensation coefficient, FN05 is applicable to a range of environmental conditions. Unlike
95 AR-G00, FN05 does not approximate functions of the maximum supersaturation and does not
96 rely on empirical relationships (except in the case of strong kinetic limitations across the CCN
97 population). A disadvantage of FN05 is that it requires iterations to solve for maximum

98 supersaturation which makes it more computationally expensive than AR-G00 (Ghan et al.
99 2011). In our global simulations, the FN05 scheme increased computational time by ~10% with
100 negligible additional increases for the FN05-based updates. A comprehensive comparison of
101 AR-G00, FN05, and several other activation parameterizations was performed by Ghan et al.
102 (2011), which showed that FN05 predicted the number fraction of activated aerosol in better
103 agreement with a high-confidence numerical solution. Despite their many differences, the
104 implementation of both AR-G00 and FN05 in CAM5.0 resulted in a small difference (0.2 W m^{-2} ,
105 10%) in the predicted effect of anthropogenic aerosol on shortwave cloud forcing (Ghan et al.,
106 2011).

107 This study expands upon the work of Ghan et al. (2011) by evaluating the individual
108 processes affecting aerosol activation within an Earth Systems Model with advanced chemistry
109 and aerosol treatments using global scale satellite/ground-base observations. Our objective is to
110 improve the model's representation of aerosol-cloud interactions by incorporating advanced
111 aerosol activation treatments into the Community Atmosphere Model version 5.1.1 within the
112 Community Earth System Model version 1.0.5 (hereto referred as CESM/CAM5) and
113 demonstrating the benefits of such advanced treatments through an initial application of the
114 improved model.

115 **2. Model Setup**

116 **2.1 CESM/CAM5 with an Advanced Aerosol Activation Module**

117 In this work, we use CESM/CAM5 to explore the impact of several different aerosol
118 activation schemes on global scale cloud properties and meteorology through aerosol-cloud
119 interactions. The CESM/CAM5 used in this work is a version recently released by NCAR and
120 further developed and improved at North Carolina State University (NCSSU) (He and Zhang,
121 2013). It includes advanced gas-phase chemistry, aerosol nucleation, and inorganic aerosol
122 thermodynamics that are coupled with the 7-mode modal aerosol module (MAM7) in CAM5
123 (Liu et al., 2012). The gas-phase chemistry is based on the 2005 Carbon Bond chemical
124 mechanism with global extension (CB05_GE) (Karamchandani et al., 2012). The aerosol
125 nucleation is based on a combination of the default nucleation parameterizations of Vehkamäki
126 et al. (2002) and (Merikanto et al., 2007) and a newly added ion-mediated aerosol nucleation
127 (Yu, 2010) above the planetary boundary layer (PBL) and the maximum nucleation rate from

128 among Vehkamäki et al. (2002), Merikanto et al. (2007), Yu (2010), and Wang et al. (2009)
129 parameterizations in the PBL (see He and Zhang (2013) for details). The inorganic aerosol
130 thermodynamics is based on ISORROPIA II (Fountoukis and Nenes, 2007), and explicitly
131 simulates thermodynamics of SO_4^{2-} , NH_4^+ , NO_3^- , Cl^- , and Na^+ as well as the impact of crustal
132 species associated with the fine dust mode. Other updates in the CESM/CAM5 version used in
133 this work include the splitting sea-salt aerosol in MAM7 into sodium and chloride to enable
134 chlorine chemistry in ISORROPIA II and addition of aqueous-phase dissolution and dissociation
135 of HNO_3 and HCl . In addition, while the released version of MAM7 uses a constant mass
136 accommodation coefficient of 0.65 for all condensable species, the NCSU's version uses species-
137 dependent accommodation coefficients for H_2SO_4 , NH_3 , HNO_3 , and HCl , with the value of 0.02,
138 0.097, 0.0024, and 0.005, respectively.

139 In the released version of CESM/CAM5, aerosol activation occurs if the liquid cloud
140 fraction either increases with time or elevation (Ghan et al., 1997; Ovtchinnikov and Ghan,
141 2005), with the number activated in the increasing cloud fraction diagnosed by the AR-G00
142 scheme as a function of aerosol chemical and physical parameters (as given by MAM7 in this
143 case), temperature, and vertical velocity (Abdul-Razzak and Ghan, 2000). Stratiform cloud
144 microphysics are described by Morrison and Gettelman (2008), which treats both the cloud
145 droplet number concentration and mixing ratio in order to simulate indirect aerosol effects and
146 cloud-aerosol interactions. A bug in the maximum supersaturation calculation in the AR-G00
147 scheme was recently reported, which has been corrected in our CESM/CAM5 simulation with
148 the AR-G00 scheme. In this work, the NCSU's version of CESM/CAM5-MAM7 is further
149 developed by providing an alternative to the AR-G00 scheme with FN05 and the updates of
150 Kumar et al. (2009) (K09) and Barahona et al. (2010) (B10) to FN05, which account for
151 adsorption activation from insoluble CCN, and giant CCN equilibrium timescale on aerosol
152 activation. In the K09 parameterization, water vapor is adsorbed onto insoluble particles such as
153 dust and black carbon (BC) whose activity is described by a multilayer Frenkel-Halsey-Hill
154 (FHH) adsorption isotherm. Calculations of the FHH adsorption isotherm in K09 account for
155 particle curvature with atmospherically-relevant adsorption parameters. Values of 2.25 and 1.20
156 are used for the A_{FHH} and B_{FHH} empirical constants, respectively (where A_{FHH} characterizes the
157 interactions of adsorbed molecules with the aerosol surface and adjacent adsorbate molecules
158 and B_{FHH} characterizes the attraction between the aerosol surface and the adsorbate in subsequent

159 layers (Kumar et al., 2009)). As insoluble adsorption leads to the activation of some particles
160 which would not easily activate under Köhler theory, a regional increase in the CDNC is
161 expected in clouds affected by high dust or BC concentrations. FHH adsorption activation
162 occurs in addition to Köhler activation in our version of CESM/CAM5, and decreases in CDNC
163 are expected to be rare. The B10 parameterization accounts for the slow condensation upon
164 inertially-limited (large) droplets in the calculation of the droplet surface area and maximum
165 supersaturation in a cloud updraft. As the slow condensation (relative to cloud formation
166 timescales) limits the activation of giant CCN, a regional decrease in the CDNC is expected in
167 clouds affected by large sea-salt aerosol and aged-dust concentrations. The simulations with the
168 FN05 scheme and updates use the same interface as that of AR-G00, with an accommodation
169 coefficient value of 0.06 (Fountoukis and Nenes, 2005) and an insoluble fraction of each mode
170 calculated from its hygroscopicity parameter (Petters and Kreidenweis, 2007).

171 **2.2 Model Simulation Design and Setup**

172 The CESM/CAM5 baseline simulations are performed using AR-G00 and FN05 for
173 aerosol activation. In addition, three sensitivity simulations are designed to test individually and
174 then collectively the impact of the aforementioned FN05-based updated parameterizations on
175 global cloud properties and radiation. During the first three simulations, FN05 is updated
176 individually by K09 and B10 (referred to as FN05/K09 and FN05/B10), respectively. The last
177 simulation contains FN05 with both updates (referred to as FN05/K09/B10). Table 1
178 summarizes all the simulations completed in this work along with their purposes. The initial
179 conditions for CAM5 are derived from a 10-yr (1990-2000) CAM5 standalone simulation with
180 the MOZART chemistry provided by NCAR. A 1-year (January 1-December 31, 2000)
181 CESM/CAM5 simulation using NCAR's CESM B_1850-2000_CAM5_CN component set is
182 performed as spinup to provide the initial conditions for meteorological variables and chemical
183 species that are treated in both MOZART and CB05_GE. All CESM/CAM5 simulations are
184 performed for the year 2001 with a 3-month (October 1-December 31, 2000) spin-up to provide
185 initial conditions for chemical species that are treated in CB05_GE but not in MOZART at a
186 horizontal grid resolution of $0.9^\circ \times 1.25^\circ$ using the B_1850-2000_CAM5_CN component set,
187 which includes all active components of CESM, 1850 to 2000 transient climate, CAM5 physics,
188 and carbon/nitrogen cycling in the Community Land Model. We selected the coupled version of
189 CESM to realistically simulate the impact of aerosol activation within an Earth Systems

190 framework. While a one-year simulation cannot determine the climate impact of aerosol
191 activation (particularly with an Earth Systems model whose components require significantly
192 longer time periods to reach equilibrium), our objective is to estimate the potential change in
193 magnitude of aerosol radiative forcing from different aerosol activation parameterizations.

194 The initial chemical conditions are based on those available in the default MOZART,
195 with missing species populated by a one-year spin-up. Anthropogenic emissions and dimethyl
196 sulfide (DMS) emissions are based on the inventory used for the global-through-urban weather
197 and forecasting model with chemistry (GU-WRF/Chem) simulations in Zhang et al. (2012) and
198 with scaled emissions of sulfur dioxide (SO₂), ammonia (NH₃), BC, and organic carbon (OC) in
199 the continental U.S., Europe, and east Asia domains based on several recent emission
200 inventories, known uncertainties in those emissions, and initial model evaluation using available
201 observations of surface chemical concentrations (He and Zhang, 2013). Online natural emissions
202 include biogenic volatile organic compounds based on the Model of Emissions of Gases and
203 Aerosols from Nature (MEGAN) scheme version 2 (Guenther et al., 2006; Heald et al., 2008),
204 dust based on the Dust Entrainment and Deposition scheme of Zender et al. (2003), and sea-salt
205 aerosol based on Mårtensson et al. (2003) for particles < 2.8 μm in dry diameter and Monahan et
206 al. (1986) for particles ≥ 2.8 μm in dry diameter.

207 **2.3 Model Evaluation Datasets and Protocol**

208 Model performance is evaluated for both radiative and meteorological predictions from
209 available surface and satellite observations for the year 2001, including aerosol optical depth
210 (AOD), CCN, CDNC, cloud fraction (CF), cloud optical thickness (COT), liquid water path
211 (LWP), shortwave cloud forcing (SWCF), downward shortwave radiation (SWDOWN),
212 downward longwave radiation (LWDOWN), outgoing longwave radiation (OLR), surface
213 precipitation (from the Global Precipitation Climatology Project) and 10 meter wind speed (from
214 the National Climatic Data Center dataset). Satellite datasets are derived from the Moderate
215 Resolution Imaging Spectroradiometer (MODIS) collection 5.1 and the Clouds and Earth's
216 Radiant Energy System (CERES) sensors aboard the Terra satellite. Global surface radiation
217 data is from the Baseline Surface Radiation Network (BSRN). In addition to the MODIS-
218 derived CDNC (Bennartz, 2007), a dataset of CDNC compiled mostly from field campaigns
219 (Karydis et al., 2011) is included. CDNC is calculated as an average value of layers between 960

220 to 850 mb for comparison with the satellite-derived values of Bennartz (2007) and is extracted
221 for the 930 mb layer (near the top of the boundary layer) for comparison with the dataset from
222 Karydis et al. (2011) and references therein. The protocols for performance evaluation follow
223 those used in Zhang et al. (2012), focusing on the annual-averaged normalized mean bias (NMB)
224 and correlation coefficient.

225 **3. Results**

226 **3.1. Global Performance Statistics**

227 Table 2 summarizes model performance statistics for aerosol, cloud, and radiative
228 predictions of CESM/CAM5 with various aerosol activation schemes over the global domain.
229 AOD is underpredicted by all simulations, with little change in the NMB (ranging from -34.0 to -
230 30.8%) and correlations (~ 0.64) among the simulations. The underprediction of AOD is likely
231 due to both underpredictions of terrestrial/anthropogenic aerosol concentrations (He and Zhang,
232 2013) and overestimates of oceanic AOD in the MODIS collection 5.1 (Levy et al., 2013). The
233 small change in AOD among the simulations is likely due to changes in meteorological
234 parameters such as surface winds and precipitation which can affect the emission, transport, and
235 lifetime of aerosols (Zhang, 2008). Although CESM-CAM5 underpredicts (NMB $< -66.7\%$)
236 column CCN concentrations at 0.5% supersaturation compared to MODIS-derived values, the
237 difficulty in using remote sensing measurements for the estimation of CCN abundances
238 (Andreae, 2009) makes interpretation uncertain.

239 CNDC, unlike AOD, is strongly influenced by the selection of aerosol activation scheme.
240 The AR-G00 simulation gives a NMB of -44.3 and -71.7% for the satellite-derived and in-situ
241 observations, respectively. For comparison, the CDNC from the FN05 simulation and all
242 sensitivity simulations with updated activation treatments is either less underpredicted or
243 becomes overpredicted with a NMB of 10.2 to 37.4% and -40.6 to -21.5% for the satellite-
244 derived and in-situ observations, respectively. The higher CDNC predicted by the FN05
245 simulation relative to AR-G00 is consistent with results from Ghan et al. (2011) and Zhang et al.
246 (2012), who attribute the difference to the tendency of the FN05 scheme to diagnose higher
247 activation fractions than the AR-G00 scheme for most environmental conditions. The higher
248 activation fraction in FN05 relative to AR-G00 is primarily due to the different values of the
249 effective uptake coefficient used in FN05 (0.06) and AR-G00 (1.0 or higher) (Zhang et al.,

250 2012). Improvement in CDNC predictions (relative to observations) from the FN05 scheme in
251 many regions is consistent with the Ghan et al. (2011) results, showing that the FN05 activated
252 fraction is more similar than that of AR-G00 to a numerical solution for marine, clean
253 continental, and background aerosol distributions for a range of updraft velocities. It should be
254 noted, however, that regions with low CDNC tend to be overestimated by the FN05 scheme.
255 Compared to the satellite-based CDNC dataset, FN05/K09 has the highest overprediction and
256 FN05/B10 has the lowest overprediction among the all FN05-based simulations. These trends
257 are expected, as insoluble adsorption in FN05/K09 leads to additional activation in regions with
258 high dust/BC concentrations while giant CCN activation kinetics leads to less activation in
259 regions with high dust/sea spray concentrations. Among the two processes (insoluble adsorption
260 and giant CCN activation kinetics) updated in the FN05 scheme, giant CCN activation kinetics in
261 FN05/B10 seems to be the most globally-significant, leading to larger changes from the FN05
262 simulation and determining the sign of CDNC predictions in the FN05/K09/B10 simulation
263 relative to FN05. Correlations between the satellite-derived/in-situ observed CDNC and
264 CESM/CAM5 predictions improve from AR-G00 to the FN05 series of simulations (with
265 correlations of 0.54 to 0.55-0.60 and -0.10 to 0.10-0.26 for the satellite-derived and in-situ
266 observations, respectively). Based on correlations, the FN05/K09/B10 simulation combining all
267 of the activation mechanism updates has the best agreement with the two CDNC datasets.

268 Changes in CDNC produced by different aerosol activation schemes have an impact on
269 the predicted cloud properties such as cloud fraction, optical thickness, liquid water path, and
270 shortwave cloud forcing. Although all model simulations predict cloud fraction very well (with
271 NMBs from -0.5 to 0.9%), there is a consistent underprediction in the mid-latitudes and tropics
272 (see Figure 1). The correlation between satellite-derived and predicted cloud fraction is
273 essentially the same for all simulations at ~ 0.71 . Significant underpredictions occur in COT
274 (with NMB of -55.6 to -40.3%) and LWP (with NMB of -75.6 to -66.8%) for all simulations (see
275 Figure 1). The COT and LWP underpredictions are consistent with those of Gettelman et al.
276 (2010) and Liu et al. (2011) who found that the predictions are most sensitive to dust loading and
277 attributed the CAM5 underpredictions to a severe underestimation of aerosol concentrations in
278 CAM5 in the Arctic (and likely Antarctic) regions. Underpredictions in COT and LWP may also
279 be caused by limitations and uncertainties associated with the microphysics modules for
280 convective clouds. For both COT and LWP, the inclusion of the FN05 scheme and updates

281 reduces the underpredictions moderately but does not improve the poor correlation (< -0.14).
282 The additional CDNC predicted by the FN05 scheme acts similarly to the impact from
283 anthropogenic aerosols; increasing the aerosol activation fraction is equivalent to adding more
284 aerosols in the calculation of cloud albedo and cloud lifetime effects. Similar to cloud fraction,
285 comparison of satellite-derived and predicted SWCF reveals that the FN05 scheme and updates
286 change the slight underprediction (with an NMB of -2.1%) for the AR-G00 simulation to
287 moderate overpredictions (with NMBs from 11.2 to 13.1%), increasing (more negative) the
288 global average SWCF by -5.0 to -5.7 W m^{-2} . Despite worsening the bias, the inclusion of the
289 FN05 updates doesn't significantly change the correlations (0.88 to 0.90). Despite having large
290 underpredictions in LWP and COT, the AR-G00 has relatively accurate predictions of
291 SWDOWN, LWDOWN, and OLR because CAM5 has been highly tuned with AR-G00 to
292 produce a small NMB for SW flux. The slight overprediction of SWDOWN and underprediction
293 and LWDOWN (with NMBs of 3.7 and -0.9% , respectively) in AR-G00 become all
294 underpredictions in the FN05 series of simulations (with NMBs of -6.1 to -5.3% and -3.0 to $-$
295 2.4%). The larger underprediction of SWDOWN in the FN05 series of simulations is likely
296 associated in part with the overprediction in CF and in part with increases in CDNC, LWP, and
297 COT. The overprediction of OLR for the AR-G00 simulation, however, is reduced by the FN05
298 series of simulations. Although the climate impact of aerosol activation cannot be determined
299 from our one-year coupled atmosphere-ocean simulations, the overprediction of precipitation and
300 underprediction of 10 meter wind speed from AR-G00 were slightly reduced (by $\sim 2\%$) in
301 FN05/K09/B10 due to small modifications of meteorology from the different activation schemes.

302 **3.2 Regional Impacts of Aerosol Activation Treatments**

303 **3.2.1 Aerosol Optical Depth and Cloud Droplet Number Concentration**

304 Like the global averages, the zonal average AOD differences between the simulations are
305 relatively insensitive (differences < 0.01) to the choice of aerosol activate schemes. Much of the
306 underprediction by all model simulations in the Southern Hemisphere from -60° to -40° is due to
307 a bias in satellite products (i.e., MODIS Collection 5.1), which does not account for the wind
308 speed-dependent whitecap and foam fraction on the ocean surface (Levy, 2013). Zonal-average
309 CDNC, on the other hand, is very sensitive to the different activation schemes. The largest
310 differences in CDNC predicted by the AR-G00 and FN05 series of simulations are in the mid-

311 latitudes (from -50° to -20° and 20° to 50°), where the AR-G00 underpredicts CDNC by 10 to 50
312 cm^{-3} and the FN05 series of simulations overpredict CDNC by 25-50 cm^{-3} compared to the
313 MODIS-derived dataset. The CDNC underprediction from the AR-G00 simulation may be
314 related in part to aerosol abundance, which is underpredicted by all of the simulations compared
315 to MODIS-derived AOD (see Figure 1) in the mid-latitudes. Like model predictions of global-
316 average CDNC, the higher zonal CDNC in the FN05 series of simulations (relative to AR-G00)
317 can be attributed to the different values of the effective uptake coefficient used in FN05 and AR-
318 G00 (Zhang et al., 2012). Among the FN05 series of simulations, the zonal-average CDNC is
319 the highest for the FN05 and FN05/K09 simulations and the lowest (closer to the MODIS-
320 derived values) for the FN05/B10 and FN05/K09/B10 simulations. The slightly higher global
321 correlation between the satellite and model predicted CDNC for the FN05/K09 and
322 FN05/K09/B10 simulations can be attributed to the higher CDNC from insoluble adsorption in
323 regions with large dust emissions (centered around -30° for deserts in southern Africa, Australia,
324 and Patagonia and 30° for the Sahara, Arabian, and Sonoran Deserts). Figure 2 shows that
325 CDNC predicted by the AR-G00 simulation is most similar to MODIS-derived CDNC over
326 oceanic regions, while the FN05 series of simulations better predict CDNC over continental
327 areas. This result is consistent with that of Figure 3a, where a comparison of field campaign-
328 observed CDNC and predictions from the AR-G00 and FN05/K09/B10 simulations reveals
329 substantial improvement in FN05/K09/B10 for continental regions which are significantly
330 underpredicted in AR-G00. The large improvement (relative to AR-G00) in continental regions
331 from the FN05/K09/B10 simulation results mainly from the higher activation fraction in the
332 FN05 scheme and larger fraction of insoluble aerosols that can be activated in the K09 scheme
333 (see Figure 3a for comparison). The overpredictions in clean marine CDNC from the FN05
334 simulation are reduced in the FN05/K09/B10 simulation (see Figure 3b) because of the inclusion
335 of giant sea-salt aerosol activation kinetics which accounts for the slow condensation of water on
336 these particles.

337 Separating the aerosol activation processes involved in the FN05/K09/B10 simulation
338 shows that the processes have unequal impacts on CDNC resulting in different spatial
339 distributions of column CDNC changes. With the inclusion of the FN05 activation scheme, most
340 areas (with the exception of desert regions in northern Africa, Arabian Peninsula, and Antarctica)
341 experience an increase in column CDNC (Figure 4). The largest increases in column CDNC

342 occur in regions near or downwind of population centers in China, U.S., and Europe. As a
343 percentage, however, the largest changes occur over the Tibetan Plateau, western U.S.,
344 Greenland, and remote Pacific Ocean where CDNC is low. Globally, the average increase in
345 CDNC from the AR-G00 simulation to the FN05 simulation is 167%. This increase is
346 substantially larger than the 20–50% increase reported by Ghan et al. (2011) for CAM5 but
347 closer in magnitude (although larger) to the 100% increase reported by Zhang et al. (2012) for
348 GU-WRF/Chem. Such differences can be attributed to differences in mass accommodation
349 coefficients of water vapor used (1.0 in AR-G00 vs. 0.06 in FN05), methods in solving max
350 supersaturation (S_{\max}) (AR-G00 uses a semi-empirical relationship to approximate S_{\max} , whereas
351 FN05 uses numerical iterations to solve S_{\max}), the temperature-dependence in the calculation of
352 Kelvin effects (temperature dependence is neglected in AR-G00 but accounted for in FN05).

353 While similar to FN05 in the magnitude of CDNC change from AR-G00, the FN05/K09
354 simulation has higher percentage changes in CDNC over many desert regions such the Saharan
355 and Arabian Deserts (see Figure 5) leading to a global average increase of 183%. This additional
356 increase is the result of insoluble CCN activating into cloud droplets that would not activate
357 according to Köhler theory on which the AR-G05 and FN05 are based. Accounting for the giant
358 CCN activation kinetics in FN05/B10 leads to smaller changes in CDNC relative to FN05,
359 especially over the remote marine and desert regions (Figure 5) where sea-salt aerosol and dust
360 are important CCN sources. Because of the large fraction of the Earth covered by oceans, the
361 FN05/B10 scheme has a globally-significant impact on average column CDNC (the average
362 increase from AR-G00 decreases from 167% in FN05 to 136% in FN05/B10). Both the
363 FN05/K09 and FN05/B10 simulations also experience isolated regions in which the CDNC
364 change is opposite to the expected (from box model simulations) trend, likely located within
365 transitional regimes as described by Reutter et al. (2009) where cloud droplet formation is
366 sensitive to both aerosol activation and updraft velocity. Combined, the effects of insoluble
367 adsorption and giant CCN activation kinetics lead to a predicted change in column CDNC from
368 the FN05 scheme that is higher than FN05 over desert regions, slightly lower over much of the
369 ocean, and relatively unchanged areas like the continental U.S., China, and Europe where either
370 the concentration of insoluble aerosols and giant CCN are low or their impacts compensate for
371 each other (see Figure 5). Compared with the AR-G00 simulation, the FN05/K09/B10
372 simulation combining all of the activation updates has a global average percent change in column

373 CDNC of 150%. With the exception of polluted regions in China, eastern Europe, and eastern
374 U.S., these changes in CDNC are greater than the internal model variability as determined by the
375 seasonal standard deviation from the AR-G00 simulation.

376 **3.2.2 Cloud Properties**

377 Unlike CDNC which is sensitive to both the implementation of the FN05 scheme and the
378 subsequent updates, changes in zonal-average cloud fraction, COT, and LWP are relatively small
379 and noticeable only by the transition from the AR-G00 to the FN05 series of simulations (see
380 Figure 1). Incremental changes are predicted for the cloud fraction predictions from different
381 aerosol activation schemes, with the largest changes occurring in the Arctic where clouds are
382 sensitive to ice nucleation (Xie et al., 2013; Engström et al., 2014). Figure 1 shows that the large
383 underpredictions in COT and LWP by AR-G00 for mid-latitude regions (30-60°N/S) are
384 significantly reduced by the implementation of the FN05 series of simulations. In tropical
385 regions, all simulations have the lowest bias in COT and LWP compared to satellite observations
386 and there exists little difference between the model simulations. The insensitivity of tropical
387 cloud properties to the various aerosol activation parameterizations is likely due to the
388 abundance of convective clouds not treated by the aerosol activation schemes and high frequency
389 of strong updrafts in the region which have been shown to have a lower variance in the activated
390 fraction from different parameterizations than do weak updrafts (Ghan et al., 2011). Predictions
391 of CF, COT, and LWP in the AR-G00 and FN05 series of simulations are most different in polar
392 regions because of the sensitivity of Arctic and Antarctic CDNC (and corresponding cloud
393 properties) to slight changes in aerosol and ice nuclei number concentration and lack of
394 sensitivity to aerosol activation treatment (Liu et al., 2011; Moore et al., 2013). Mixed-phase
395 clouds, which are found in polar regions, are particularly difficult to simulate because they are
396 affected by both aerosol activation and ice nucleation (Lance et al., 2011; Xie et al., 2013).
397 Ignoring polar regions which have mixed-phase clouds, the moderate underpredictions of CF,
398 COT, and LWP in the AR-G00 are consistently reduced in the FN05 series of simulations.

399 Changes in cloud fraction, COT, and LWP affect the potential climatic impact of
400 aerosols, as shown by the changes in SWCF (see Figures 1 and 4). The difference in SWCF
401 between the AR-G00 and FN05 simulations is the highest in the mid-latitudes where the large
402 CDNC differences occur. In mid-latitude regions from -60° to -30°, the transition from the AR-
403 G00 to the FN05 activation schemes changes the sign of the model bias from negative to positive

404 (see Figure 1). Globally, the largest changes in SWCF between the AR-G00 and FN05
405 simulations occur over the oceans, where widespread areas experience a 25% increase (larger by
406 10 W m^{-2} in magnitude) in SWCF (see Figure 4). This sensitivity of radiative forcing in oceanic
407 regions to aerosol activation is due to two main reasons: 1) the low penetration of shortwave
408 radiation through stratocumulus decks covering large areas of the ocean and 2) the sensitivity of
409 marine cloud albedo to changes in CDNC (Twomey, 1991; Platnick and Twomey, 1994; Moore
410 et al., 2013). The updates to the FN05 scheme do not substantially affect the spatial distribution
411 of SWCF changes relative to the change from AR-G00 to FN05. Because the various Earth
412 System components of CESM interact in our simulations, these predicted changes in cloud
413 properties (which are statistically significant with a probability value from a student's t-test \ll
414 0.05) cannot be entirely attributable to aerosol activation. A significantly longer simulation time
415 period and/or prescribed ocean surface conditions are needed to reduce the impact of ocean-
416 atmosphere-cloud feedbacks existing in our simulations.

417 **4. Conclusions**

418 In this study, several process-based aerosol activation schemes are implemented into the
419 Community Atmosphere Model version 5.1.1 within the Community Earth System Model
420 version 1.0.5 (CESM/CAM5) to determine the global impacts of individual activation processes
421 on cloud properties. Compared to simulations using the default Abdul-Razzak and Ghan (2000)
422 aerosol activation parameterization, simulations with the Fountoukis and Nenes (2005) scheme
423 and updates for insoluble aerosol adsorption (Kumar et al., 2009) and giant cloud condensation
424 nuclei (CCN) activation kinetics (Barahona et al., 2010) are slower (~10% increase in
425 computational time) but have improved predictions of cloud droplet number concentration
426 (CDNC), cloud optical thickness, and liquid water path in many regions. The inclusion of these
427 updates leads to a widespread large increase in CDNC with localized enhancement of CDNC
428 over desert regions and depression of CDNC over oceanic regions. The increase in CDNC
429 predicted by the simulations with updated aerosol activation results in a decrease (more negative)
430 in the global-average shortwave cloud forcing and surface shortwave radiation. In regions where
431 these physically-based updates lead to more accurate prediction of CDNC, cloud optical
432 thickness, and liquid water path, we have increased confidence in the predicted magnitude of the
433 radiative forcing from aerosol-cloud interactions. While this study estimates the impact of
434 aerosol activation on cloud properties within an Earth Systems model, determining the climate

435 impact requires a longer simulation period and more comprehensive treatments of aerosol-cloud
436 interactions. Future studies on the interaction between aerosol activation and cloud microphysics
437 could be improved through the direct coupling of convection and aerosol activation (Song et al.,
438 2012), inclusion of entrainment on aerosol activation (Barahona and Nenes, 2007), modification
439 of the Nenes and Seinfeld (2003) population splitting concept (Morales Betancourt and Nenes,
440 2014), and by simulating longer time periods to allow for the various components of the Earth
441 Systems model to approach equilibrium.

442 **Acknowledgements**

443 This project is sponsored by the National Science Foundation EaSM program (AGS-
444 1049200). AN acknowledges support from DOE EaSM and NASA MAP grants. Thanks are
445 due to R. Bennartz, Department of Atmospheric and Oceanic Sciences, University of Wisconsin-
446 Madison, for providing derived CDNC data derived based on MODIS measurements. The
447 GPCP combined precipitation data were developed and computed by the NASA/Goddard Space
448 Flight Center's Laboratory for Atmospheres as a contribution to the GEWEX Global
449 Precipitation Climatology Project. We would like to acknowledge high-performance computing
450 support from Yellowstone (ark:/85065/d7wd3xhc) provided by NCAR's Computational and
451 Information Systems Laboratory, sponsored by the National Science Foundation. We also
452 acknowledge Steven Ghan and the anonymous reviewer for their helpful and insightful
453 comments.

454

455 **References**

- 456 Abdul-Razzak, H., Ghan, S., and Rivera-Carpio, C.: A parameterisation of aerosol activation.
457 Part I: Single aerosol type, *J. Geophys. Res.*, 103, 6123–6132, doi:10.1029/97JD03735,
458 1998.
- 459 Abdul-Razzak, H. and Ghan, S. J.: A parameterization of aerosol activation: 2. Multiple aerosol
460 types, *J. Geophys. Res.*, 105, 6837–6844, 2000.
- 461 Albrecht, B. A.: Aerosols, cloud microphysics, and fractional cloudiness, *Science*, 245(4923),
462 1227–1230, doi:10.1126/science.245.4923.1227, 1989.
- 463 Andreae, M. O.: Correlation between cloud condensation nuclei concentration and aerosol
464 optical thickness in remote and polluted regions, *Atmos. Chem. Phys.*, 9, 543-556,
465 doi:10.5194/acp-9-543-2009, 2009.

466 Barahona, D. and Nenes, A.: Parameterization of cloud droplet formation in large-scale models:
467 including effects of entrainment, *J. Geophys. Res.*, 112, D16206,
468 doi:10.1029/2007JD008473, 2007.

469 Barahona, D., West, R. E. L., Stier, P., Romakkaniemi, S., Kokkola, H., and Nenes, A.:
470 Comprehensively accounting for the effect of giant CCN in cloud activation
471 parameterizations, *Atmos. Chem. Phys.*, 10, 2467–2473, doi:10.5194/acp-10-2467-2010,
472 2010.

473 Bennartz, R.: Global assessment of marine boundary layer cloud droplet number concentration
474 from satellite, *J. Geophys. Res.-Atmos.*, 112, D02201, doi:10.1029/2006JD007547, 2007.

475 Boucher, O., Randall, D., Artaxo, P., Bretherton, C., Feingold, G., Forster, P., Kerminen, V.-M.,
476 Kondo, Y., Liao, H., Lohmann, U., Rasch, P., Satheesh, S.K., Sherwood, S., Stevens, B., and
477 Zhang, X.Y.: Clouds and Aerosols. In: *Climate Change 2013: The Physical Science Basis.*
478 Contribution of Working Group I to the Fifth Assessment Report of the Intergovernmental
479 Panel on Climate Change [Stocker, T.F., D. Qin, G.-K. Plattner, M. Tignor, S.K. Allen, J.
480 Boschung, A. Nauels, Y. Xia, V. Bex and P.M. Midgley (eds.)]. Cambridge University Press,
481 Cambridge, United Kingdom and New York, NY, USA, 2013.

482 Chuang, P. Y., Charlson, R. J., and Seinfeld, J. H.: Kinetic limitations on droplet formation in
483 clouds, *Nature*, 390, 594–596, doi:10.1038/37576, 1997.

484 Engström, A., Karlsson, J., and Svensson, G.: , The importance of representing mixed-phase
485 clouds for simulating distinctive atmospheric states in the Arctic, *J. Clim.*, 27, 265–272,
486 2014.

487 Fountoukis, C. and Nenes, A.: Continued development of a cloud droplet formation
488 parameterization for global climate models, *J. Geophys. Res.*, 110, D11212,
489 doi:10.1029/2004jd005591, 2005.

490 Gettelman, A., Liu, X., Ghan, S. J., Morrison, H., Park, S., Conley, A. J., Klein, S. A., Boyle, J.,
491 Mitchell, D. L., and Li, J. L. F.: Global simulations of ice nucleation and ice supersaturation
492 with an improved cloud scheme in the Community Atmosphere Model, *J. Geophys. Res.*,
493 115, D18216, doi:10.1029/2009jd013797, 2010.

494 Ghan, S. J., Leung, L. R., Easter, R. C., and Abdul-Razzak, H.: Prediction of droplet number in a
495 general circulation model, *J. Geophys. Res.*, 102, 21777–21794, 1997.

496 Ghan, S. J., Abdul-Razzak, H., Nenes, A., Ming, Y., Liu, X., Ovchinnikov, M., Shipway, B.,
497 Mekhidze, N., Xu, J., and Shi, X.: Droplet nucleation: Physically-based parameterizations
498 and comparative evaluation, *J. Adv. Model. Earth Syst.*, 3, M10001,
499 doi:10.1029/2011MS000074, 2011.

500 Guenther, A., Karl, T., Harley, P., Wiedinmyer, C., Palmer, P. I., and Geron, C.: Estimates of
501 global terrestrial isoprene emissions using MEGAN (Model of Emissions of Gases and
502 Aerosols from Nature), *Atmos. Chem. Phys.*, 6, 3181-3210, doi:10.5194/acp-6-3181-2006,
503 2006.

504 He, J. and Zhang, Y.: Improvement and further development in CESM/CAM5: gas-phase
505 chemistry and inorganic aerosol treatments, *Atmos. Chem. Phys. Discuss.*, 13, 27717-27777,
506 doi:10.5194/acpd-13-27717-2013, 2013.

507 Heald, C. L., Henze, D. K., Horowitz, L. W., Feddema, J., Lamarque, J. F., Guenther, A., Hess,
508 P. G., Vitt, F., Seinfeld, J. H., Goldstein, A. H., and Fung, I.: Predicted change in global
509 secondary organic aerosol concentrations in response to future climate, emissions, and land
510 use change, *J. Geophys. Res.-Atmos.*, 113, D05211, doi:10.1029/2007JD009092, 2008.

511 Karamchandani, P., Zhang, Y., Chen, S. Y., and Balmori-Bronson, R.: Development and testing
512 of an extended chemical mechanism for global through-urban applications, *Atmos. Pollut.*
513 *Res.*, 3(1), 1–24, doi:10.5094/APR.2011.047, 2012.

514 Karydis, V. A., Kumar, P., Barahona, D., Sokolik, I. N., and Nenes, A.: On the effect of dust
515 particles on global cloud condensation nuclei and cloud droplet number, *J. Geophys. Res.*,
516 116, D23204, doi:10.1029/2011jd016283, 2011.

517 Khain, A. P., BenMoshe, N., and Pokrovsky, A.: Factors determining the impact of aerosols on
518 surface precipitation from clouds: An attempt at classification, *J. Atmos. Sci.*, 65, 1721–
519 1748, 2008.

520 Köhler, H.: The nucleus in the growth of hygroscopic droplets, *T. Faraday Soc.*, 32, 1152-1161,
521 1936.

522 Kumar, P., Sokolik, I. N., and Nenes, A.: Parameterization of cloud droplet formation for global
523 and regional models: including adsorption activation from insoluble CCN, *Atmos. Chem.*
524 *Phys.*, 9, 2517–2532, doi:10.5194/acp-9-2517-2009, 2009.

525 Lance, S., Shupe, M. D., Feingold, G., Brock, C. A., Cozic, J., Holloway, J. S., Moore, R. H.,
526 Nenes, A., Schwarz, J. P., Spackman, J. R., Froyd, K. D., Murphy, D. M., Brioude, J.,
527 Cooper, O. R., Stohl, A., and Burkhardt, J. F.: Cloud condensation nuclei as a modulator of ice
528 processes in Arctic mixed-phase clouds, *Atmos. Chem. Phys.*, 11, 8003-8015,
529 doi:10.5194/acp-11-8003-2011, 2011.

530 Leaitch, W. R., Isaac, G. A., Strapp, J. W., Banic, C. M., and Wiebe, H. A.: The relationship
531 between cloud droplet number concentrations and anthropogenic pollution: Observations and
532 climatic implications, *J. Geophys. Res.*, 97, 2463–2474, doi:10.1029/91JD02739, 1992.

533 Levy, R. C., Mattoo, S., Munchak, L. A., Remer, L. A., Sayer, A. M., Patadia, F., and Hsu, N.
534 C.: The Collection 6 MODIS aerosol products over land and ocean, *Atmos. Meas. Tech.*, 6,
535 2989-3034, doi:10.5194/amt-6-2989-2013, 2013.

536 Liu, X., Xie, S., Boyle, J., Klein, S. A., Shi, X., Wang, Z., Lin, W., Ghan, S. J., Earle, M., Liu, P.
537 S. K., and Zelenyuk, A.: Testing cloud microphysics parameterizations in NCAR CAM5
538 with ISDAC and M-PACE observations, *J. Geophys. Res.*, 116, D00T11,
539 doi:10.1029/2011JD015889, 2011.

540 Liu, X., Easter, R. C., Ghan, S. J., Zaveri, R., Rasch, P., Shi, X., Lamarque, J.-F., Gettelman, A.,
541 Morrison, H., Vitt, F., Conley, A., Park, S., Neale, R., Hannay, C., Ekman, A. M. L., Hess,
542 P., Mahowald, N., Collins, W., Iacono, M. J., Bretherton, C. S., Flanner, M. G., and Mitchell,
543 D.: Toward a minimal representation of aerosols in climate models: description and
544 evaluation in the Community Atmosphere Model CAM5, *Geosci. Model Dev.*, 5, 709-739,
545 doi:10.5194/gmd-5-709-2012, 2012.

546 Mårtensson, E., Nilsson, E., de Leeuw, G., Cohen, L., and Hansson, H.-C.: Laboratory
547 simulations and parameterisation of the primary marine aerosol production, *J. Geophys. Res.*,
548 108, 4297, doi:10.1029/2002JD002263, 2003.

549 Martin, G. M., Johnson, D. W., and Spice, A.: The measurement and parameterization of
550 effective radius of droplets in warm stratocumulus clouds, *J. Atmos. Sci.*, 51, 1823-1842,
551 1994.

552 Merikanto, J., Napari, I., Vehkamäki, H., Anttila, T., and Kulmala, M.: New parameterization of
553 sulfuric acid-ammonia-water ternary nucleation rates at tropospheric conditions, *J. Geophys.*
554 *Res.*, 112, D15207, doi:10.1029/2006JD007977, 2007.

555 Monahan, E., Spiel, D., and Davidson, K.: A model of marine aerosol generation via white caps
556 and wave disruption, in: *Oceanic whitecaps*, edited by: Monahan, E. and MacNiocaill, G.,
557 167–193, Dordrecht: Reidel, The Netherlands, 1986.

558 Moore, R. H., Karydis, V. A., Capps, S. L., Latham, T. L., and Nenes, A.: Droplet number
559 uncertainties associated with CCN: an assessment using observations and a global model
560 adjoint, *Atmos. Chem. Phys.*, 13, 4235-4251, doi:10.5194/acp-13-4235-2013, 2013.

561 Morales Betancourt, R. and Nenes, A.: Droplet activation parameterization: the population
562 splitting concept revisited, *Geosci. Model Dev. Discuss.*, 7, 2903-2932, doi:10.5194/gmdd-7-
563 2903-2014, 2014.

564 Morrison, H. and Gettelman, A.: A new two-moment bulk stratiform cloud microphysics scheme
565 in the Community Atmosphere Model, Version 3 (CAM3), part I: description and numerical
566 tests, *J. Climate*, 21, 3642–3659, doi:10.1175/2008JCLI2105.1, 2008.

567 Nenes, A., Ghan, S., Abdul-Razzak, H., Chuang, P. Y., and Seinfeld, J. H.: Kinetic limitations on
568 cloud droplet formation and impact on cloud albedo, *Tellus B*, 53, 133–149,
569 doi:10.1034/j.1600-0889.2001.d01-12.x, 2001.

570 Nenes, A. and Seinfeld, J. H.: Parameterization of cloud droplet formation in global climate
571 models, *J. Geophys. Res.*, 108, 4415, doi:10.1029/2002jd002911, 2003.

572 Ovtchinnikov, M. and Ghan, S. J.: Parallel simulations of aerosol influence on clouds using
573 cloud-resolving and single-column models, *J. Geophys. Res.*, 110, D15S10,
574 doi:10.1029/2004JD005088, 2005.

575 Petters, M. D. and Kreidenweis, S. M.: A single parameter representation of hygroscopic growth
576 and cloud condensation nucleus activity, *Atmos. Chem. Phys.*, 7, 1961-1971,
577 doi:10.5194/acp-7-1961-2007, 2007.

578 Platnick, S. and S. Twomey: Determining the susceptibility of cloud albedo to changes in droplet
579 concentration with the advanced very high resolution radiometer, *J. Appl. Meteorol.*, 33,
580 334–347, doi:10.1175/1520-0450(1994)033<0334:DTSOCA>2.0.CO;2, 1994.

581 Ramanathan, V., Crutzen, P. J., Kiehl, J. T., and Rosenfeld, D.: Aerosols, Climate, and The
582 Hydrological Cycle, *Science*, 294, 2119–2124, doi:10.1126/science.1064034, 2001.

583 Rosenfeld, D., Lohmann, U., Raga, G. B., O’Dowd, C. D., Kulmala, M., Fuzzi, S., Reissell, A.,
584 and Andreae, M. O., Flood or drought: How do aerosols affect precipitation?, *Science*, 321,
585 1309–1313, 2008.

586 Reutter, P., Su, H., Trentmann, J., Simmel, M., Rose, D., Gunthe, S. S., Wernli, H., Andreae, M.
587 O., and Pöschl, U.: Aerosol- and updraft-limited regimes of cloud droplet formation:
588 influence of particle number, size and hygroscopicity on the activation of cloud condensation
589 nuclei (CCN), *Atmos. Chem. Phys.*, 9, 7067-7080, doi:10.5194/acp-9-7067-2009, 2009.

590 Song, X., Zhang, G. J., and Li J.-L. F.: Evaluation of microphysics parameterization for
591 convective clouds in the NCAR Community Atmosphere Model CAM5, *J. Clim.*, 25, 8568–
592 8590, 2012.

593 Twomey, S.: Pollution and the planetary albedo, *Atmos. Environ.*, 8, 1251–1256,
594 doi:10.1016/0004-6981(74)90004-3, 1974.

595 Twomey, S.: Influence of pollution on shortwave albedo of clouds, *J. Atmos. Sci.*, 34(7), 1149–
596 1152, doi:10.1175/1520-0469(1977)034,1149:TIOPOT.2.0.CO;2, 1977.

597 Twomey, S.: Aerosols, clouds and radiation, *Atmos. Environ.*, 25A, 2435–2442,
598 doi:10.1016/0960-1686(91)90159-5, 1991.

599 Vehkamäki, H., Kulmala, M., Napari, I., Lehtinen, K. E. J., Timmreck, C., Noppel, M., and
600 Laaksonen, A.: An improved parameterization for sulfuric acid water nucleation rates for
601 tropospheric and stratospheric conditions, *J. Geophys. Res.*, 107, 4622–4632,
602 doi:10.1029/2002JD002184, 2002.

603 Wang, M., Penner, J. E., and Liu, X.: Coupled IMPACT aerosol and NCAR CAM3 model:
604 Evaluation of predicted aerosol number and size distribution, *J. Geophys. Res.*, 114, D06302,
605 doi:10.1029/2008JD010459, 2009.

606 Xie, S., Liu, X., Zhao, C., Zhang, Y.: Sensitivity of CAM5-simulated arctic clouds and radiation
607 to ice nucleation parameterization. *J. Climate*, 26, 5981–5999, doi:10.1175/JCLI-D-12-
608 00517.1, 2013.

609 Yang, B., Qian, Y., Lin, G., Leung, L-Y, Rasch, P. J., Zhang, G. J., McFarlane, S. A., Zhao, C.,
610 Zhang, Y., Wang, H., Wang, M., Liu, X.: Uncertainty quantification and parameter tuning in
611 the CAM5 Zhang-McFarlane convection scheme and impact of improved convection on the
612 global circulation and climate, *J. Geophys. Res. Atmos.*, 118, 395–415,
613 doi:10.1029/2012JD018213, 2013.

614 Yu, F.: Ion-mediated nucleation in the atmosphere: Key controlling parameters, implications,
615 and look-up table, *J. Geophys. Res.*, 115, D03206, doi:10.1029/2009JD012630, 2010.

616 Zender, C., Bian, H., and Newman, D.: Mineral Dust Entrainment and Deposition (DEAD)
617 model: Description and 1990s dust climatology, *J. Geophys. Res.*, 108, 4416–4437,
618 doi:10.1029/2002jd002775, 2003.

619 Zhang, G. J. and McFarlane, N. A.: Sensitivity of climate simulations to the parameterization of
620 cumulus convection in the Canadian Climate Centre general circulation model, *Atmos.*
621 *Ocean*, 33, 407–446, 1995.

622 Zhang, Y.: Online-coupled meteorology and chemistry models: history, current status, and
623 outlook, *Atmos. Chem. Phys.*, 8, 2895-2932, doi:10.5194/acp-8-2895-2008, 2008.

624 Zhang, Y., Karamchandani, P., Glotfelty, T., Streets, D. G., Skamarock, W. C., Grell, G., Nenes,
625 A., Yu, F., and Bennartz, R.: Development and initial application of the Global-Through-
626 Urban Weather Research and Forecasting Model with Chemistry (GU-WRF/Chem), *J.*
627 *Geophys. Res.*, 117, D20206, doi:10.1029/2012JD017966, 2012.

Table 1. The CESM/CAM5-MAM7 simulations performed in this study.

Name	Köhler activation	Population spitting	Insoluble adsorption	Giant CCN equilibrium	Major Differences and Purpose
AR-G00	✓				Baseline simulation
FN05	✓	✓			Uses the Fountoukis and Nenes [2005] activation scheme
FN05/K09	✓	✓	✓		Uses the Fountoukis and Nenes [2005] activation scheme updated by Kumar et al. [2009], accounting for the impact of insoluble adsorption
FN05/B10	✓	✓		✓	Uses the Fountoukis and Nenes [2005] activation scheme updated by Barahona et al. [2010], accounting for the impact of giant CCN activation kinetics
FN05/K09/B10	✓	✓	✓	✓	Uses the Fountoukis and Nenes [2005] activation scheme updated by Kumar et al. [2009], and Barahona et al. [2010], accounting for all above aerosol activation processes

Table 2. Annual mean normalized mean biases (NMBs, in %) of the CESM-CAM5-predicted meteorological/radiative variables.

Variable	Dataset	AR-G00	FN05	FN05/K09	FN05/B10	FN05/K09/B10
AOD	MODIS	-33.9	-32.3	-31.7	-30.8	-31.6
CCN	MODIS	-66.7	-80.6	-80.9	-81.2	-81.2
CDNC	Bennartz (2007)	-44.3	28.0	37.4	10.2	16.0
	Karydis et al. (2011)	-69.2	-23.5	-21.5	-40.6	-24.4
CF	MODIS	-0.5	0.5	0.9	0.7	0.0
COT	MODIS	-55.6	-41.1	-40.3	-43.0	-41.9
LWP	MODIS	-75.6	-66.9	-66.8	-67.8	-67.2
SWCF	CERES	-2.1	13.0	13.1	11.3	11.2
SWDOWN	BSRN	3.7	-5.3	-6.1	-5.4	-5.3
LWDOWN	BSRN	-0.9	-3.0	-2.5	-2.4	-2.5
OLR	NOAA-CDC	3.2	2.2	2.2	2.3	2.5
Precipitation	GCPC	11.3	8.5	8.7	8.9	9.3
Wind Speed	NCDC	-16.1	-15.2	-14.7	-14.8	-14.2

Table 3. Annual mean correlation coefficients of the CESM-CAM5-predicted meteorological/radiative variables.

Variable	Dataset	AR-G00	FN05	FN05/K09	FN05/B10	FN05/K09/B10
AOD	MODIS	0.66	0.65	0.65	0.65	0.66
CCN	MODIS	0.49	0.37	0.37	0.37	0.37
CDNC	Bennartz (2007)	0.54	0.55	0.58	0.55	0.58
	Karydis et al. (2011)	-0.10	0.16	0.24	0.10	0.26
CF	MODIS	0.71	0.72	0.71	0.71	0.71
COT	MODIS	-0.17	-0.16	-0.15	-0.14	-0.14
LWP	MODIS	-0.38	-0.37	-0.37	-0.36	-0.36
SWCF	CERES	0.88	0.90	0.89	0.90	0.90
SWDOWN	BSRN	0.90	0.91	0.91	0.90	0.90
LWDOWN	BSRN	0.98	0.97	0.98	0.98	0.98
OLR	NOAA-CDC	0.97	0.97	0.97	0.97	0.97
Precipitation	GCPC	0.80	0.76	0.77	0.78	0.79
Wind Speed	NCDC	0.40	0.41	0.41	0.41	0.41

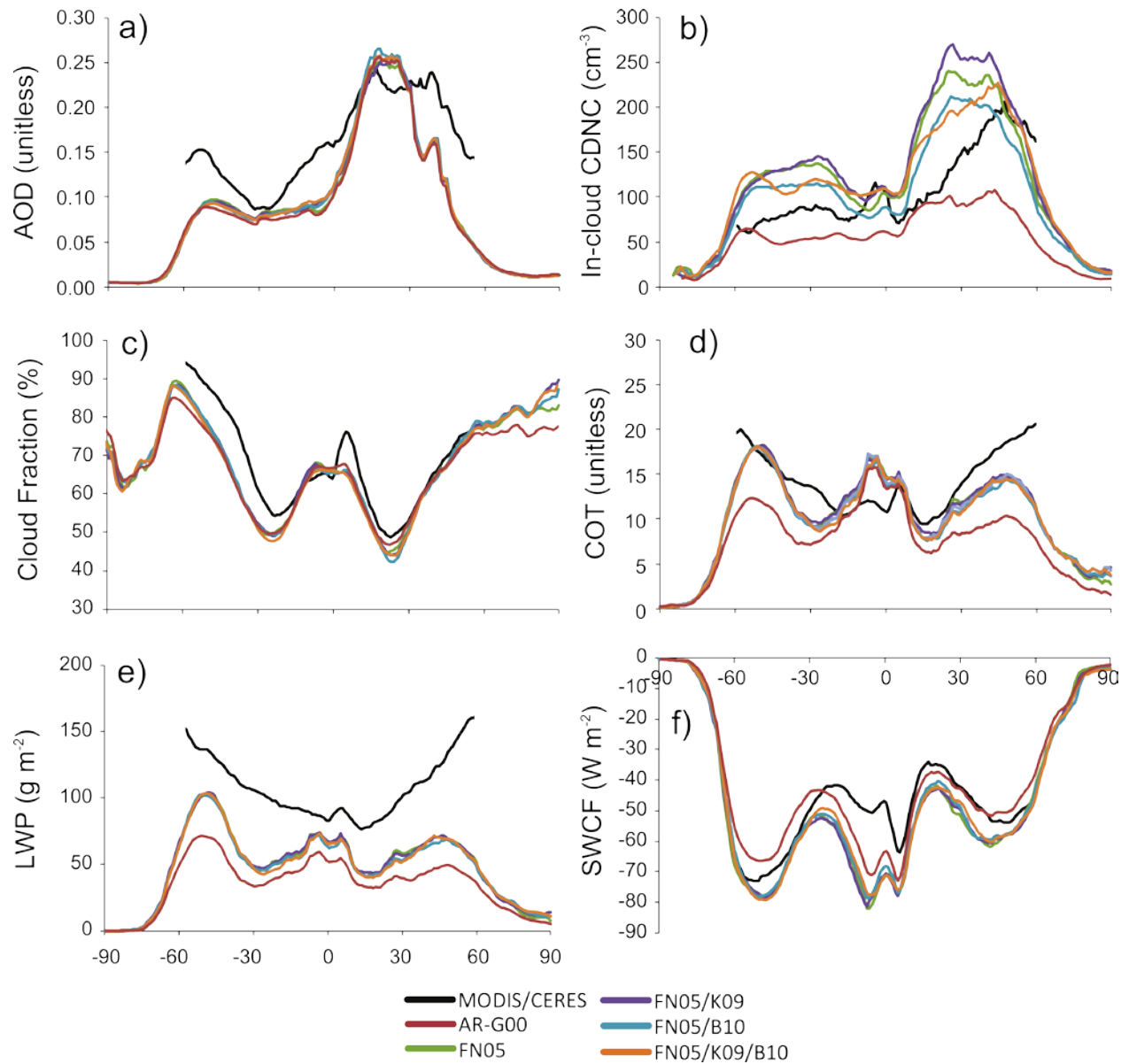


Figure 1. Annual-average zonal-mean a) aerosol optical depth, b) low level cloud droplet number concentration (MODIS values derived from Bennartz (2007) and CESM/CAM5 values averaged between 960 and 850 mb), c) cloud fraction, d) cloud optical thickness, e) liquid water path, and f) shortwave cloud forcing derived from satellites and predicted by CESM/CAM5.

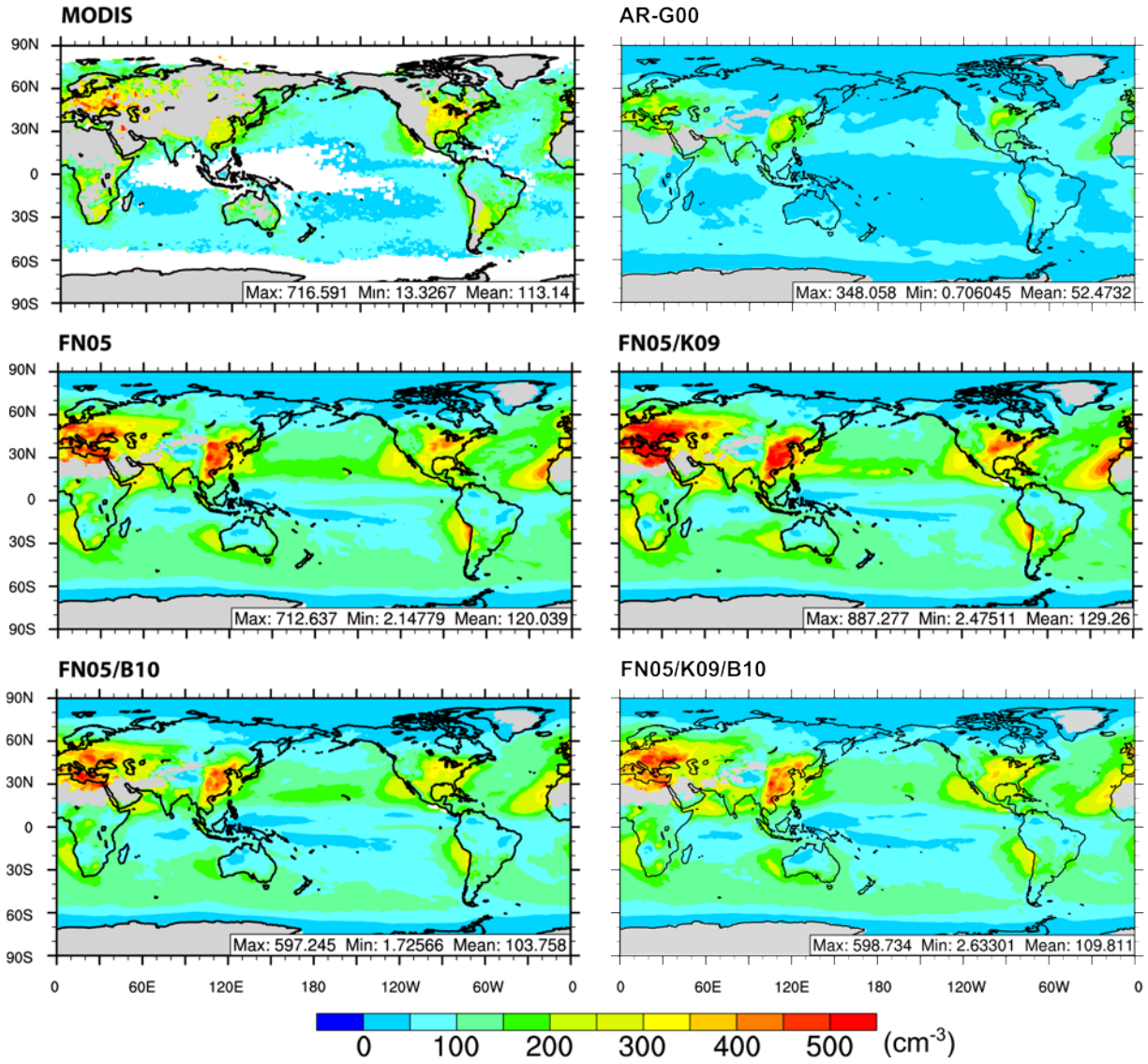


Figure 2. Annual average low-level CDNC from MODIS (Bennartz, 2007) and CESM/CAM5 (averaged between 960 to 850 mb) simulations.

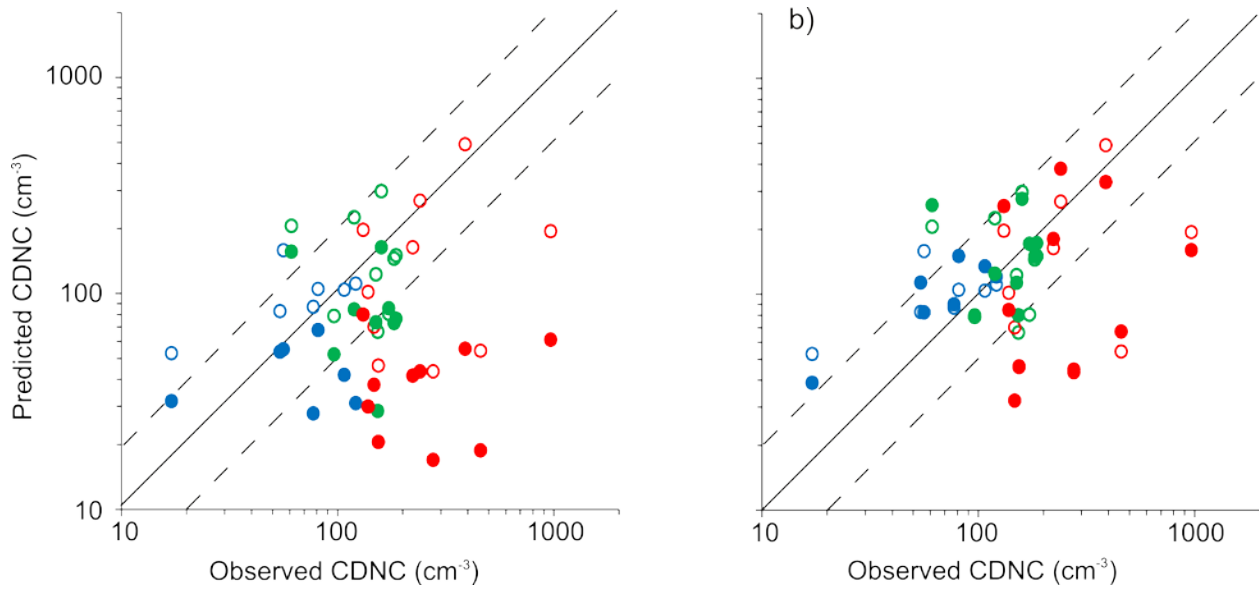
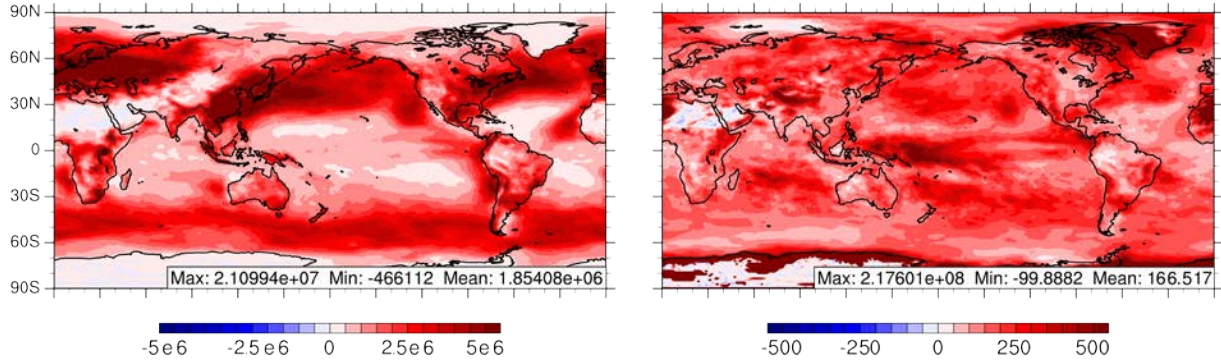


Figure 3. Comparison of CEM5/CAM5-predicted (at ~930 mb) and observed low-level CDNC from field campaigns in clean marine (blue), polluted marine (green), and continental (red) environments as classified and summarized by Karydis et al. (2011). The filled circles are for the (a) AR-G00 and (b) FN05 simulations and hollow circles for the FN05/K09/B10 simulation. Data points where predicted CDNC < 10 cm^{-3} were not included. The 1:1 and 1:2/2:1 lines are the solid and dotted black lines, respectively.

Column CDNC (left: cm^{-2} , right: %)



Shortwave Cloud Forcing (left: W m^{-2} , right: %)

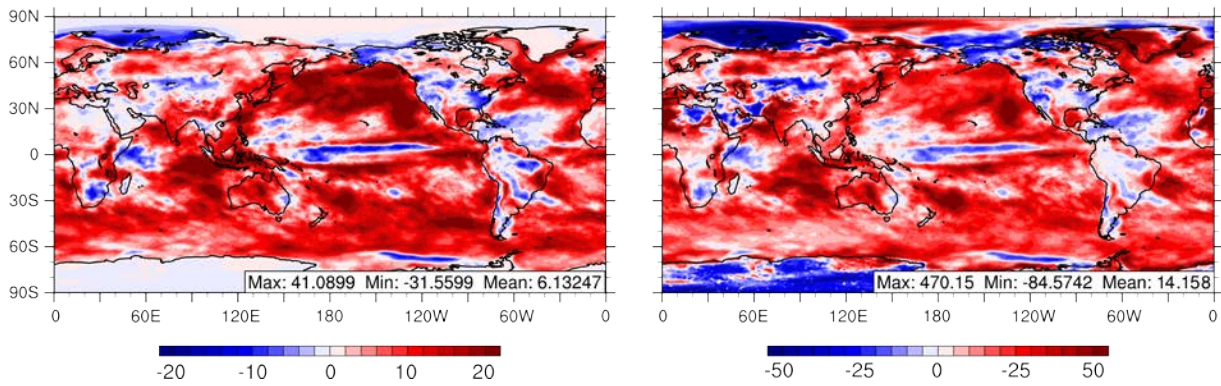


Figure 4. Annual-average absolute and percentage changes from the FN05 and AR-G00 CESM/CAM5 simulations for column CDNC and shortwave cloud forcing. Because the shortwave cloud forcing typically has negative values, the absolute change map (bottom left) uses $|\text{SWCF}|$ so that the warmer colors represent an increase in the forcing even though they are more negative values. The global mean percentage change values are calculated from the averaged absolute change rather than the average of the gridded percentage changes.

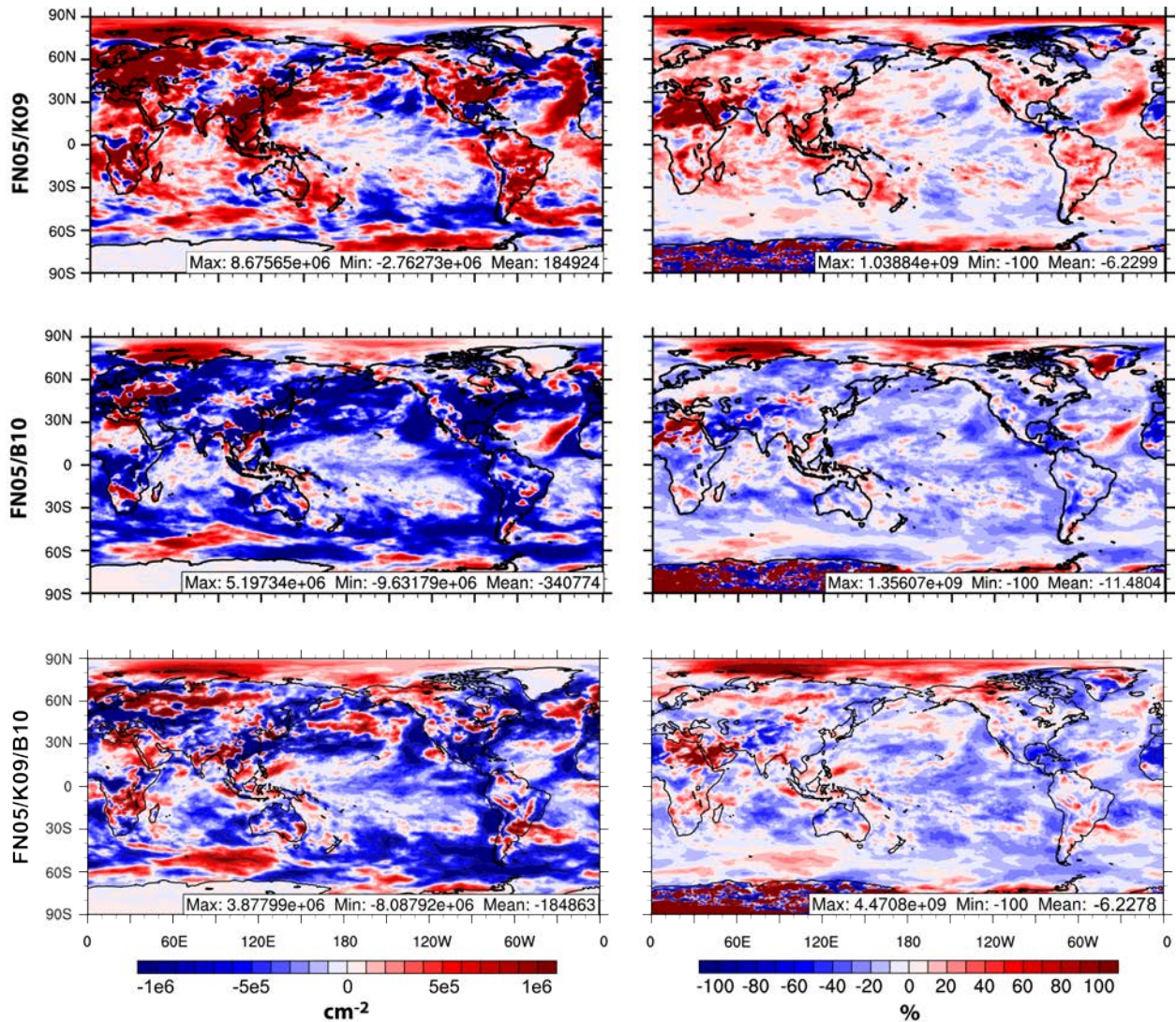


Figure 5. Annual-average absolute (left, in units of cm^{-2}) and percentage (right) change in column CDNC from FN05 to each of the FN05 updates in CESM/CAM5. The global mean percentage change values are calculated from the averaged absolute change rather than the average of the gridded percentage changes. Note that the color bar range for the left column is a factor of 5 less than that of Figure 4 (top left) to better show spatial details.